# Power Generation Potential of SC-$CO_2$ Thermosiphon for Engineered Geothermal Systems

Alvin I. Remoroza*, Elham Doroodchi, Behdad Moghtaderi
[1]Priority Research Centre for Energy, School of Engineering (Chemical Eng.), Faculty of Engineering & Built Environment, University of Newcastle
University Drive, Callaghan, NSW 2308, Australia
* Corresponding author: Alvin.Remoroza@studentmail.newcastle.edu.au

Numerical modelling was conducted to assess thermodynamic properties and power generation potential of SC-$CO_2$ thermosiphon for Engineered Geothermal Systems (EGS) and compared with $H_2O$-based EGS with Organic Rankine Cycle (ORC).

*Keywords*: SC-$CO_2$ thermosiphon, Enhanced Geothermal System, Hot Dry Rock

## Findings from the Simulation

The methodology and reference data (Table 1) adopted in this paper is similar to that used by Atrens et al (2009) for computing the overall flow in an EGS. The calculations are divided into two parts, injection and production sections. The injection calculations include fluid well-bore flow from the surface to the bottom of the injection well and fluid flow through the reservoir. The production calculations only include fluid well-bore flow from the bottom of the production well to the surface.

The following sets of equations with the assumptions of adiabatic flow and negligible kinetic energy at the wellbore, and reservoir Darcy flow of constant cross-sectional area (single channel flow) with linearly increasing temperature were used in the injection calculation;

$$P_{inj} = P_{res} + \Delta P_{f,well} + \Delta P_{f,res} - \rho g \Delta z$$

$$\Delta P_{f,well} = f \frac{\Delta z}{D} \rho \frac{V^2}{2} = f 8 \frac{\Delta z \dot{m}^2}{\pi^2 \rho D^5}$$

$$f = \left[ -1.8 \log \left( \frac{6.9}{\mathrm{Re}} + \left[ \frac{\varepsilon}{3.7D} \right]^{1.11} \right) \right]^{-2}$$

$$\Delta P_{f,res} = \frac{\dot{m} \mu \Delta L}{\rho \kappa A}$$

In the production section, the adiabatic flow defines the following relationship,

$$P_{prod} = P_{res} - \rho g \Delta z - \Delta P_{f,well}$$

Where $V$ = fluid velocity

$\dot{m}$ = mass flow rate

$f$ = friction factor

$\rho$ = density

$$\mathrm{Re} = \frac{\rho V D}{\mu} = \frac{4\dot{m}}{\mu \pi D}$$

$\varepsilon$ = pipe roughness

$D$ = pipe diameter

$g$ = gravitational constant, 9.81 m/s$^2$

$\kappa$ = homogenous permeability

$A$ = swept area of the fluid flow in the reservoir

$P_{inj}$ = injection pressure

$P_{res}$ = reservoir pressure at the bottom of the production well

$\Delta P_{f,well}$ = frictional losses at the well

$\Delta P_{f,res}$ = reservoir pressure losses

$\Delta L$ = incremental reservoir length

$\Delta z$ = incremental vertical distance

The total exergy generated from SC-$CO_2$ thermosiphon EGS was dominated by exergy associated with change in enthalpy. The specific exergy can be expressed as

$$X_H = (h - h_0) - T_0 (S - S_0)$$

Where $X_H$ = exergy associated with change in enthalpy

$h$ = specific enthalpy

$S$ = specific entropy

$T$ = temperature in Kelvin

The subscript 0 denotes initial conditions.

Numerical simulations were carried out using Engineering Equation Solver (EES). EES calculates thermodynamic properties for carbon dioxide using the fundamental equation of state developed by Span and Wagner (1996) and viscosity and thermal conductivity based on the work by Vesovic et al (1990). EES gives thermodynamic properties of water using the 1995

Formulation for the Thermodynamic Properties of Ordinary Water Substance for General and Scientific Use issued by The International Association for the Properties of Water and Steam (IAPWS).

Table 1: Reference values used in the exergy analysis

| Parameter | Values (Artens, 2009) | Values (this study) |
|---|---|---|
| Reservoir Length | 1000 m | 1000 m |
| Reservoir Temperature | 225$^0$C | 225$^0$C |
| Reinjection Temperature | 25$^0$C | 25$^0$C |
| kA (inverse impedance) | 2.1E-19 m$^4$ | 2.1E-19 m$^4$ |
| Reservoir Pressure, $P_{res}$ | Hydrostatic (49.05MPa) | Hydrostatic (49.05MPa) |
| Wellbore Roughness ( $\varepsilon$ ) | 400 micrometer | 400 and 40 micrometer |
| Wellbore Diameter, $D$ | 0.2315 | 0.2315 |
| Reference Temperature | 25$^0$C | 25$^0$C |

### Effect of Pipe Roughness

Pipe frictional losses at the injection well are higher for SC-$CO_2$ than for $H_2O$ because pipe roughness affects $CO_2$ mass flow rates more than it affect $H_2O$ mass flow (Figures 1 and 2).

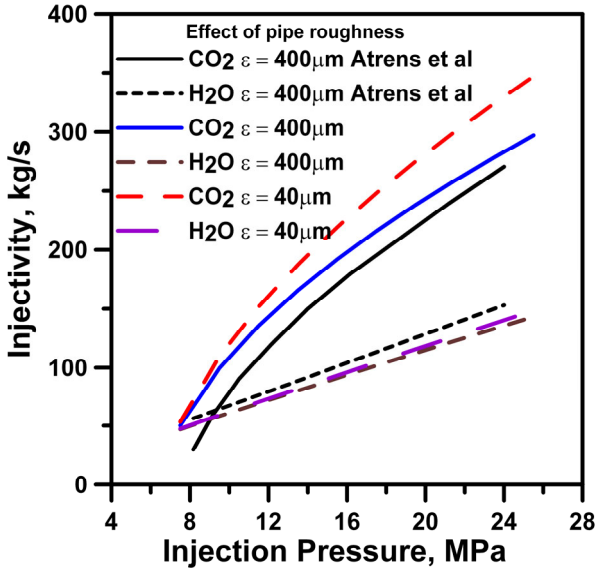


Figure 1: Injectivity of SC-$CO_2$ and water at different injection pressures and roughness values.

Bottomhole pressures at the injection well with $H_2O$ circulation are, in theory, greater than with SC-$CO_2$ circulation because (a) $H_2O$ has higher density than $CO_2$ at the same pressure-temperature conditions, and (b) $CO_2$ has higher pipe frictional losses than water for the same mass flow rate. Reservoir pressure losses are significantly higher for $H_2O$ than SC-$CO_2$ thermosiphon based system because of $H_2O$'s higher kinematic viscosity ($\mu/\rho$) at the given T-P domain in the reservoir (plots not shown).

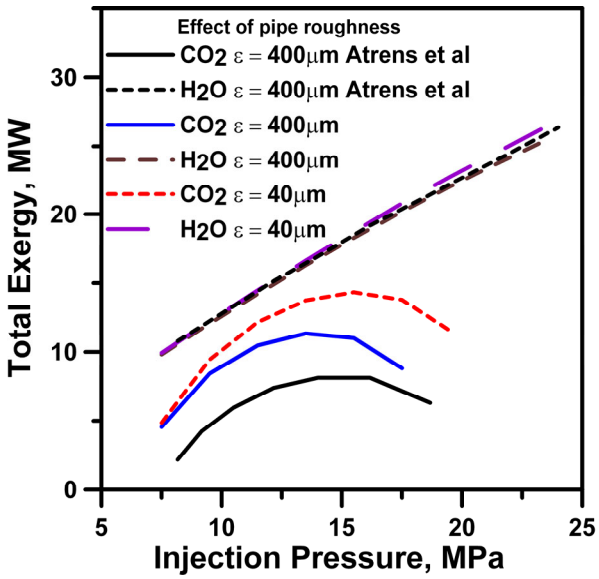


Figure 2: Total exergy provided by SC-$CO_2$ and water at different injection pressures and roughness values.

### Pressure and Temperature Well Profile of the Injection Well

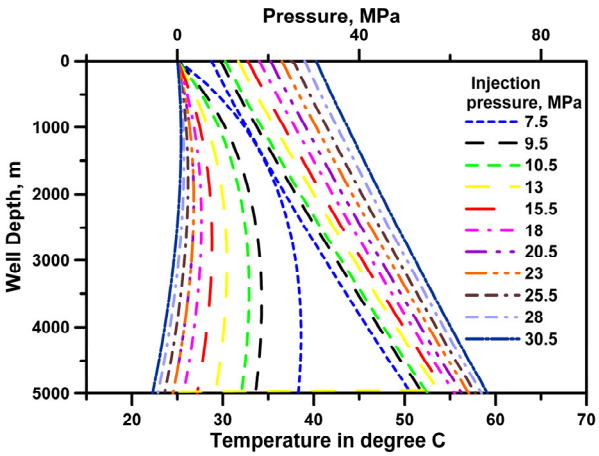


Figure 3: Temperature (left plots, lower X-axis) and pressure (right plots, upper X-axis) well profile at the SC-$CO_2$ injection well (Note: pipe roughness used is 40 microns).

For SC-$CO_2$ adiabatic flow at the injection well, the SC-$CO_2$ temperature at the bottom may be higher (at lower injection pressure) or lower (at higher injection pressure) than the injection temperature (Figure 3). Specific enthalpy of SC-$CO_2$ is affected by temperature and pressures whereas specific enthalpy of $H_2O$ is affected by temperature and only slightly by pressure (Pruess; 2006, 2008).

### Effect of Injection Temperature

Injection temperature affects SC-$CO_2$ and $H_2O$ in somewhat different ways (Figure 4);

- For SC-$CO_2$, lowering the injection temperature increases the pipe frictional and reservoir losses due to increased

density and viscosity. However, the gain in the pressure head (i.e. increase in bottomhole pressure) due to increased density is far more than the total losses resulting in net overall gain in buoyant force driving natural convection.

- For $H_2O$, decreasing the injection temperature actually decreases the pipe frictional losses, slightly increases bottomhole pressure and increases reservoir pressure losses. Overall, reservoir losses are greater than the combined head gain and less pipe frictional losses resulting in slight decrease in injectivity.

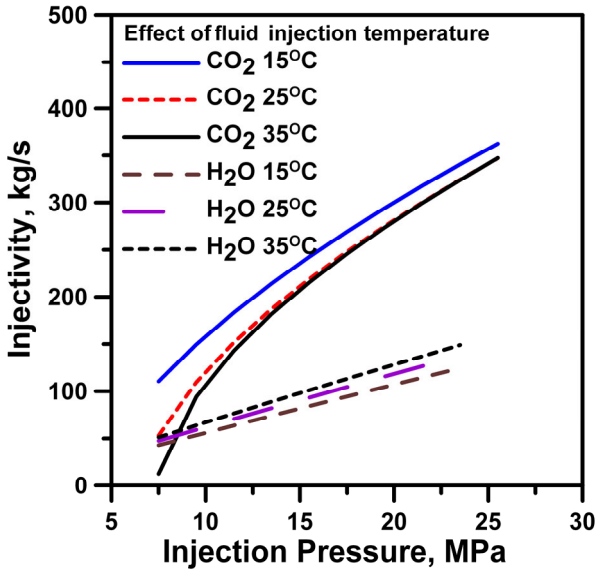


Figure 4: Effect of injection temperature on injectivity.

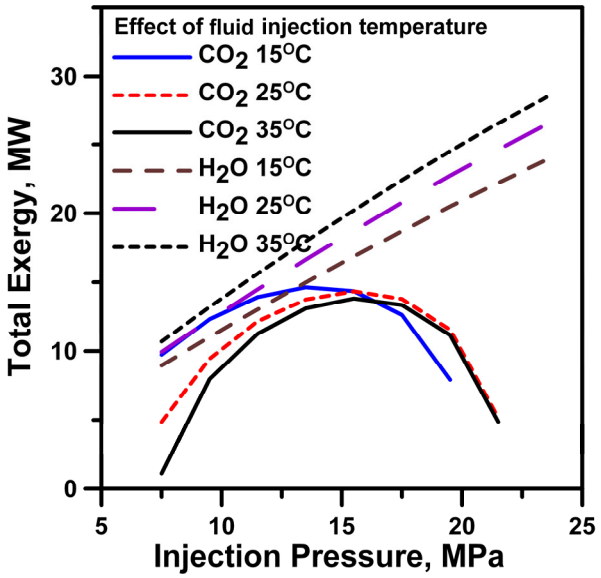


Figure 5: Effect of reinjection pressure and temperature on total exergy.

Whenever reinjection temperature of $15^0$C or less are possible, SC-$CO_2$ thermosiphon based EGS can have slightly higher thermal heat extraction efficiency at injection pressures lower than ~13.0 MPa (Figure 5).

## Single Channel versus Radial Reservoir Flow

Radial pressure distribution in the reservoir from an injection well can be described in the following equation

$$P(r) = \frac{\mu \dot{V}}{2\pi K L_R} \ln(r)$$

Where $\mu$ = absolute viscosity

$\dot{V} = m/\rho$ = volumetric flow rate of the fluid

$K$ = homogenous permeability

$L_R$ = reservoir depth or thickness

The pressure difference between the injection well face, $r_W$ and the production well located at distance, $r_R$ (equals 1000 m in our previous assumptions) can be approximated using the following equation

$$\Delta P_{f,well} = \frac{\mu * \dot{m}}{2 * \pi * \rho * K * L_R} \ln(\frac{r_W}{r_R})$$

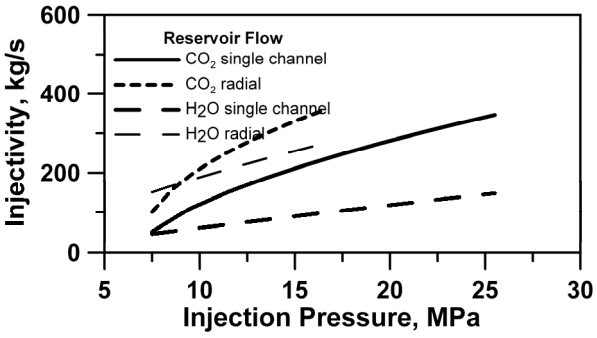


Figure 6: Effect of reservoir flow model choice on injectivity.

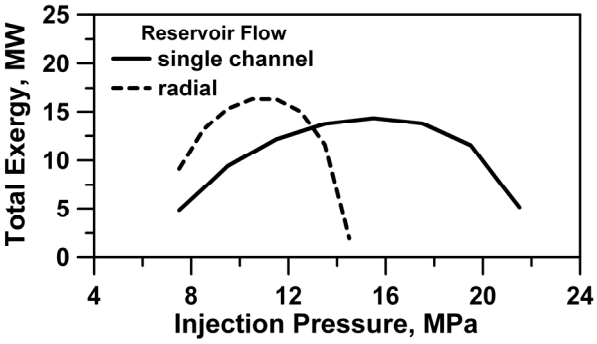


Figure 7: Effect of reservoir flow model choice in total exergy of a SC-$CO_2$ thermosiphon EGS.

Comparing single channel (constant cross-sectional area, i.e. pipe flow) and radial reservoir flow showed that radial reservoir flow gives higher injectivity and consequently improved total exergy (Figures 6 and 7). This behaviour is due to lower

reservoir pressure losses in radial reservoir flow compared to single channel flow.

### Sensitivity of Exergy to Well-Configuration

Well configuration (ratio of the number of injection to production wells) does not significantly affect the injectivity of the fluid but it affects the performance of the production wells. Higher number of production wells lowers the frictional losses because of lower mass flow rates in each well since the mass flow rate of the circulating fluid is equally divided by the number of production wells. For single channel reservoir flow, 1 injection to 2 production well ratio gives the optimum total exergy while the five-spot well configuration (1 injection to 4 production well ratio) gives the optimum total exergy for radial reservoir flow. On the basis of per drilled well (sum of injection and production wells), the doublet configuration (1 injection to 1 production well) gives the highest total exergy both for single channel and radial reservoir flow (Figures 8 and 9).

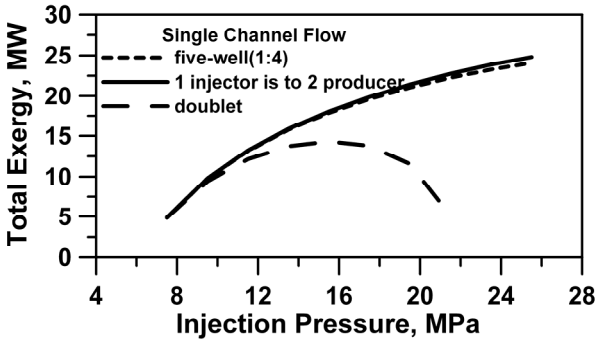


Figure 8: Effect of well configuration on total exergy of SC-$CO_2$ on single channel reservoir flow.

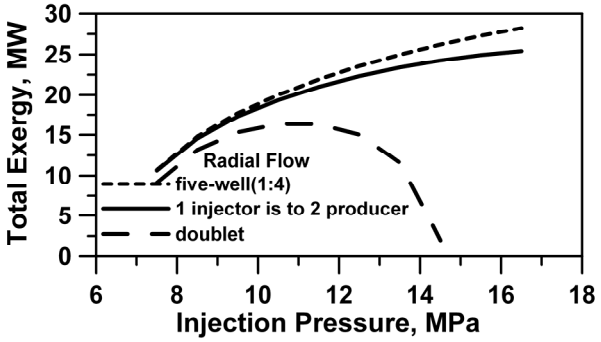


Figure 9: Effect of well configuration on total exergy of SC-$CO_2$ on radial reservoir flow.

It can be deduced that if five-spot well-configuration is used, the radial reservoir flow model would be more appropriate to implement in numerical modelling. Doublet and 1 injection to 2 production well configurations would command the implementation of single channel reservoir flow modelling. Based on the results, doublet configuration is the most efficient in extracting heat based on the total exergy per drilled well.

### $H_2O$-based EGS with Organic Rankine Cycle versus SC-$CO_2$ Thermosiphon Power Cycle Analysis

$H_2O$ based EGS can not be used in a thermosiphon power cycle since the production pressure is always lower than the injection pressure.

In SC-$CO_2$ power cycle analysis, the gross potential electrical power is calculated based on $CO_2$ isentropic expansion in the turbine with 85% turbine efficiency (Figure 10). Temperature-entropy diagram of a SC-$CO_2$ power cycle at injection pressure of 7.5 MPa is given in Figure 11. It shows that super-critical $CO_2$ exists in all stages of the process. Auxiliary power requirement is not included in the calculations, i.e. power used in cooling tower, etc. It is assumed that no pump will be used in the SC-$CO_2$ thermosiphon power cycle.

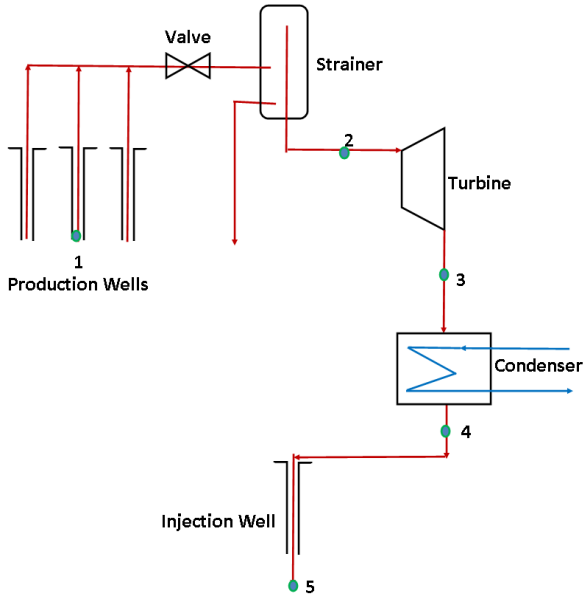


Figure 10: Schematic Diagram of a SC-$CO_2$ Thermosiphon Power Cycle.

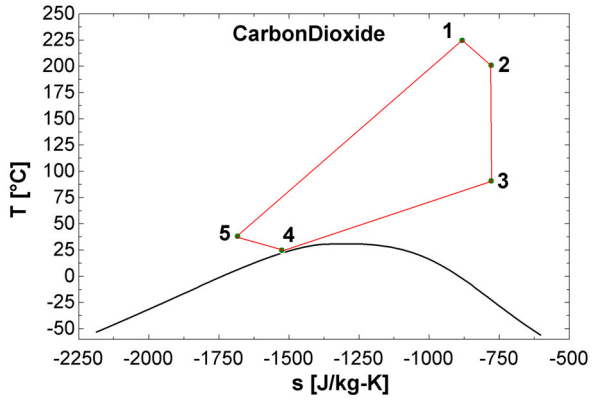


Figure 11 Temperature-entropy diagram of SC-$CO_2$ thermosiphon power cycle.

Power cycle analysis of $H_2O$-based EGS ORC (Figure 12) assumes the use of isopentane as the secondary fluid with circulating pump pressure of 2.793 MPa ($T_{sat}$ = 175$^0$C) and condenser pressure of 101.325 kPa (atmospheric condition). This circulation pump pressure is chosen so that existence of two-phase is avoided during expansion at the turbine while giving the maximum power (Figure 13). The pump is assumed to be 75% efficient and isentropic.

The power generated from $H_2O$ based EGS with ORC is calculated as turbine power minus pump power for $H_2O$ injection and circulation of the working fluid and does not include power used in the cooling tower and other auxiliary equipment.

$$W = W_{turbine} - W_{injection} - W_{ORC,circulation}$$

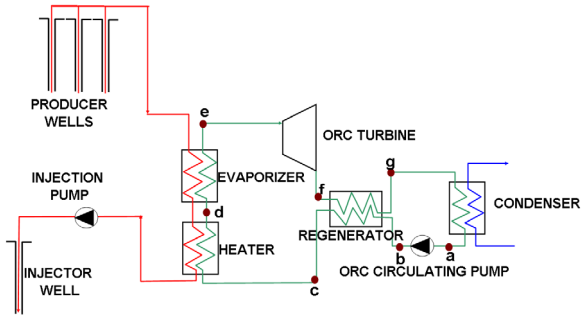


Figure 12: Schematic diagram of binary organic rankine cycle for $H_2O$ based EGS.

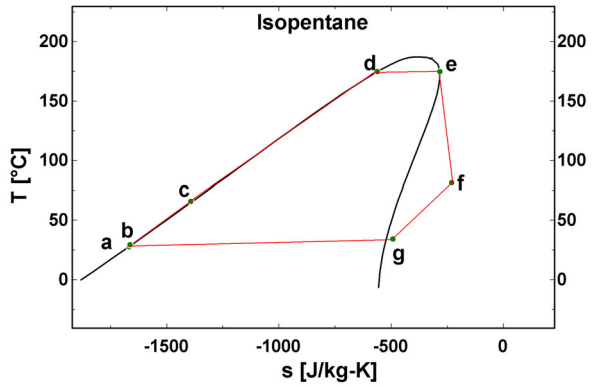


Figure 13: Temperature-entropy diagram of ORC with Isopentane as working fluid.

Power cycle analysis showed that $H_2O$ based EGS is better in mining heat and transferring that heat in secondary fluids for electrical power generation than SC-$CO_2$ thermosiphon EGS (it maybe different for pump $CO_2$ EGS because of possible higher injectivity). The optimum power that can be generated from SC-$CO_2$ thermosiphon is 8.6 MW at 9.5 MPa injection pressure at radial reservoir flow model while for $H_2O$-based EGS with ORC, the electrical power potential at the same conditions is 25.8 MW. For single channel reservoir flow model, the optimum electrical power potential of a SC-$CO_2$ thermosiphon is 6.3 MW while for $H_2O$-based EGS is 9.4 MW. Electrical power potential of $H_2O$-based EGS linearly increases with injection pressure whereas for SC-$CO_2$ thermosiphon EGS the relationship is parabolic (see Figure 14).

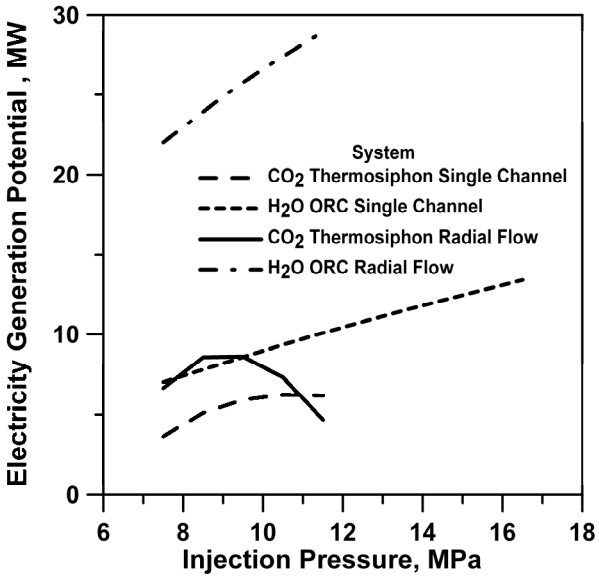


Figure 14: Potential electricity generation comparison of a SC-$CO_2$ thermosiphon and $H_2O$ based EGS with ORC (assumes 85% turbine efficiency and 75% pump efficiency).

The less number of equipment of a SC-$CO_2$ thermosiphon power cycle (no injection pump and circulation pump for secondary fluid) and relative inertness of $CO_2$ with regards to rock-interaction and associated mineral dissolution, precipitation and fouling of equipment warrant further evaluation. However, SC-$CO_2$ thermosiphon power cycle will require research and development of SC-$CO_2$ turbine.

### Sensitivity of Exergy to Reservoir Depth

The performance of SC-$CO_2$ thermosiphon EGS on shallower hot dry rock geothermal resource was also investigated. The numerical simulation used single channel reservoir flow model and doublet well configuration, the same resource temperature of 225$^0$C and injection temperature of 25$^0$C, and changing well depth to 3000 m and assuming reservoir pressure at the producer well to 29.43MPa (assumes hydrostatic pressure).

The over-all effect of shallower reservoir depth of the HDR geothermal resource at SC-$CO_2$ thermosiphon EGS were lower total exergy and lower electricity generation potential due to lower production pressures (Figures 15 and 16). However, SC-$CO_2$ injectivity increased at shallower HDR geothermal resource depth. The total exergy of $H_2O$-based EGS increased at deeper reservoir depth but the electricity generation potential were similar.

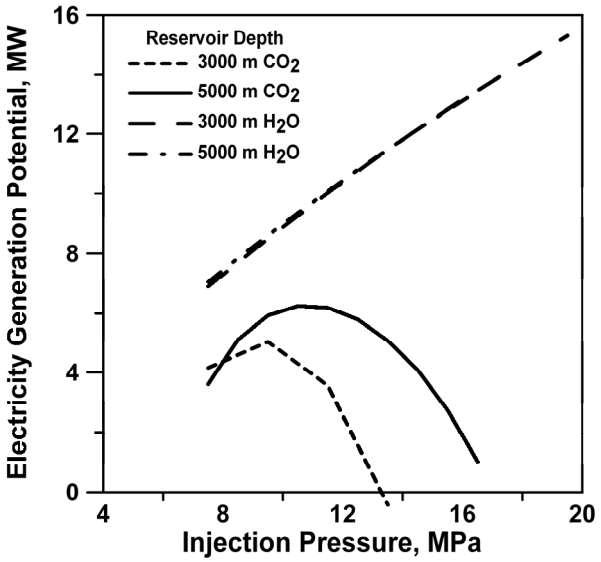


Figure 15: Effect of reservoir depth on SC- $CO_2$ thermosiphon on electricity generation potential (assumes 85% turbine efficiency).

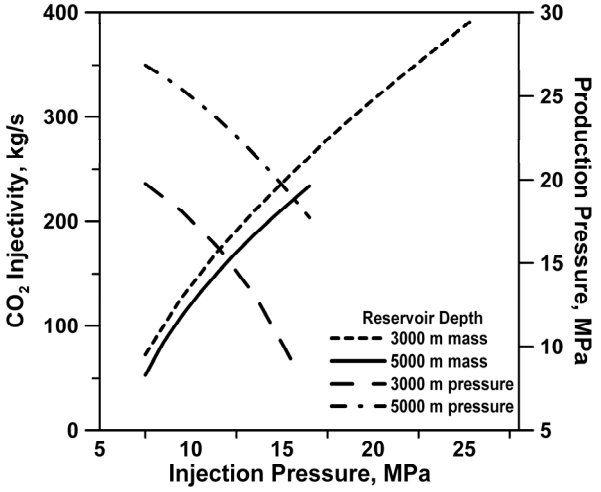


Figure 16: Effect of reservoir depth on SC-$CO_2$ thermosiphon on injectivity and production pressure.

## Recommendations

The less complicated design of CS-$CO_2$ thermosiphon EGS and relative inertness of $CO_2$ with regards to rock-interaction and associated mineral dissolution, precipitation and fouling of equipment warrant further economic and geochemical evaluation. Research and development of high efficiency SC-$CO_2$ turbine is also necessary to prove the viability of this system. The use of pump for SC-$CO_2$ circulation in EGS may also be investigated.

Economic and thermodynamic analyses over the full life of SC-$CO_2$ and $H_2O$ based EGS should be carried out to compare their overall environmental and economic performances. One can determine the total amount of $CO_2$ that will be created and sequestered plus the amount of conventional $CO_2$ emissions that will be avoided during the entire life cycle of CS-$CO_2$ thermosiphon and $H_2O$ EGS projects. It appears from this study that $H_2O$ based EGS can generate more electrical power than CS-$CO_2$ thermosiphon EGS.

The amount of $CO_2$ that may be sequestered and stored in a SC-$CO_2$ thermosiphon EGS is only an added ancillary benefit since the amount is negligible compared to the current total $CO_2$ emission. Another concern will be the issue of possible $CO_2$ leakage in EGS.

This paper merely present the results of a thermodynamic and power cycle analysis, it does not prove or disprove the viability of using SC-$CO_2$ circulation EGS.

## References

Atrens, A. D., Gurgenci, h. and Rudolph, V. (2008). Carbon Dioxide Thermosiphon Optimisation, in: Gurgenci, H. and Budd, A.R. (eds.), Proceedings of the Sir Mark Oliphant International Frontiers of Science and Technology Australian Geothermal Energy Conference, Geoscience Australia, Record 2008/12,149-152.

Atrens, A. D., H. Gurgenci, and V. Rudolph (2009). $CO_2$ Thermosiphon for Competitive Geothermal Power Generation. Energy & Fuels 23(1): 553-557.

Atrens, A. D., H. Gurgenci, and V. Rudolph (2009). EXERGY ANALYSIS OF A $CO_2$ THERMOSIPHON. PROCEEDINGS, Thirty-Fourth Workshop on Geothermal Reservoir Engineering, Stanford University, Stanford, California.

Pruess, K. (2006). Enhanced geothermal systems (EGS) using $CO_2$ as working fluid - A novel approach for generating renewable energy with simultaneous sequestration of carbon. Geothermics 35(4): 351-367.

Pruess, K. (2008). On production behavior of enhanced geothermal systems with $CO_2$ as working fluid. Energy Conversion & Management 49(6): 1446-1454.

Pruess, K. and M. Azaroual (2006). On the feasibility of using supercritical $CO_2$ as heat transmission fluid in an engineered hot dry rock geothermal system. PROCEEDINGS, Thirty-First Workshop on Geothermal Reservoir Engineering, Stanford University, Stanford, California.

Span, R. and W. Wagner (1996). A New Equation of State for Carbon Dioxide Covering the Fluid Region from the Triple-Point Temperature to 1100 K at Pressures up to 800 MPa. J. Phys. Chem. Ref. Data 25: 1509-96.

Vesovic, V., W. A. Wakeham, G. A. Olchowy, J. V. Sengers, J. T. R. Watson, and J. Millat (1990). The Transport Properties of Carbon Dioxide. J. Phys. Chem Ref. Data 19(3): 763-808.